Journal of Wind Engineering & Industrial Aerodynamics 169 (2017) 177–193

Contents lists available at ScienceDirect

Journal of Wind Engineering & Industrial Aerodynamics

journal homepage: www.elsevier.com/locate/jweia

CFD simulation of CO_2 dispersion from urban thermal power plant: Analysis of turbulent Schmidt number and comparison with Gaussian plume model and measurements

Francisco Toja-Silva [a,*], Jia Chen [a], Stephan Hachinger [b], Frank Hase [c]

[a] Environmental Sensing and Modeling (ESM), Technische Universität München (TUM), Theresienstr. 90, 80333 Munich, Germany
[b] Leibniz Supercomputing Centre (Leibniz-Rechenzentrum, LRZ) of the Bavarian Academy of Sciences and Humanities, Boltzmannstr. 1, 85748 Garching, Germany
[c] Institute of Meteorology and Climate Research, Karlsruher Institut für Technologie (KIT), Postfach 3640, 76021 Karlsruhe, Germany

ARTICLE INFO

Keywords:
CFD
Column-averaged dry-air mole fraction measurement
Pollutant dispersion
Gaussian plume model
OpenFOAM
Urban areas

ABSTRACT

This investigation presents computational fluid dynamics (CFD) simulations of carbon dioxide (CO_2) dispersion from a natural gas-fueled thermal power plant in an urban environment. The results are compared with experimental measurements of column-averaged dry-air mole fraction (XCO_2) on the site, obtaining a good agreement. Different turbulent Schmidt numbers are compared, and we suggest a value for being used in full-scale simulations. The particular characteristics, e.g. azimuth and elevation angles of the XCO_2 measurement, are analyzed and taken into account for the comparison with simulation results. The conclusions from this comparison are useful not only for the XCO_2 experimental data analysis, but also for the efficient and successful design of future measurement campaigns. The simulation results are also compared with the Gaussian plume model, and a new parametrization (i.e. vertical dispersion parameter) is suggested for being used in the urban environment. Additionally, CO_2 concentration maps for an urban area are presented, and the spatial distribution is analyzed.

1. Introduction

Climate change, a societal challenge for the European Union, is affecting all regions and has a profound impact on society and environment. A wide range of consequences are expected in the future, potentially causing high costs (European Environmental Agency, 2012). Between 1980 and 2011, floods affected more than 5.5 million people and caused direct economic losses of more than 90 billion of Euros (European Commission). It is now evident that the present global warming period is due to the strong anthropogenic greenhouse gas (GHG) emission, occurring at a rate unprecedented in the past 66 million years (Zeebe et al., 2016). Therefore, the identification and control of the greenhouse gas sources has a great relevance. Since the GHG emissions from cities and power plants are the largest human contribution to climate change (NASA), the present investigation focuses on this environment. Most of the countries compile an annual emission inventory (IPCC's). However, a rigorous approach requires to perform GHG measurements in order to verify the official estimates. The resulting GHG emission estimation will serve several practical purposes (Gurney et al., 2015), e.g. the verification of emission inventories and the determination of trends in urban emissions (McKain et al., 2012), the ability to make targeted and financially efficient decisions about mitigation options (Gurney, 2013), and the identification and avoidance of unintentional and furtive releases (e.g. from leaking gas pipes (McKain et al., 2015) or malfunctioning gas facilities).

GHG concentration measurements were carried out using aircrafts (Karion et al., 2013; Mays et al., 2009), but this technique is unfeasible for an everyday real-time monitoring system. Measurements of GHG concentration at the ground level (Yue et al., 2016) and measurements of column-averaged dry-air mole fraction of CO_2 (XCO_2) (Hase et al., 2015; Chen et al., 2016) can be carried out continuously at single points. However, these instruments capture the GHG concentration on the air, but not the GHG rate emitted by the source. Therefore, these punctual measurement data need to be extended to the surrounding urban map in order to comprehensively detect and quantify GHG emission sources, being required a deep understanding of the gas transport and diffusion phenomena. The numerical simulation of the physical problem yields the relationship between the emission rate and the concentration value that can be measured. Whereas the emission rate must be known for the simulation, after a validation using measurements on the site (as in the

* Corresponding author.
E-mail address: f.toja@tum.de (F. Toja-Silva).

http://dx.doi.org/10.1016/j.jweia.2017.07.015
Received 13 March 2017; Received in revised form 20 July 2017; Accepted 22 July 2017

present investigation), further simulations can be used in order to reproduce multiple real scenarios without the necessity of a real event (it can be called numerical experiment). Such numerical experiments can be carried out for training machine learning algorithms (Leuenberger and Kanevski, 2015; Lary et al., 2016) (i.e. simpler models), that can be integrated into the measurement devices in order to predict the source origin and emission rate using single measurements on the site. The simulation results also yield GHG concentration maps that are very useful for designing future measurement campaigns. As demonstrated in the present article, the GHG emission from a power plant cannot be detected by a ground measurement close to the power plant, and a sensor network should not be arbitrarily designed for obtaining reasonably good results.

The Weather Research and Forecasting (WRF) model (Beck et al., 2011) is commonly used for the simulation at the meso-scale. It reaches a grid resolution of around 1 km (Feng et al., 2016). In order to thoroughly understand emissions, it is however also necessary to map them on a finer scale (micro-scale simulations), reflecting the dimensions at which carbon is emitted: by individual buildings, vehicles, parks, factories and power plants.

With this aim, this investigation presents a completely new approach to the analysis of the CO_2 emissions from fossil fuel thermal power plants in urban environments. We combine differential column measurements (Chen et al., 2016) with computational fluid dynamics (CFD) simulations. Several researchers have developed CFD simulations for dealing with pollutants dispersion in urban areas using wind tunnel models (e.g. (Takano and Moonen, 2013; Tominaga and Stathopoulos, 2010; Hang et al., 2012; Tang et al., 2006; Tominaga and Stathopoulos, 2007; Yu and Thé, 2016; Gromke and Blocken, 2015; Zhang et al., 2015; Wingstedt et al., 2017)), and less investigations have dealt with real cities (e.g. (Nozu and Tamura, 2012; Patnaik et al., 2007; Jeanjean et al., 2015; Hanna et al., 2006)). Some review articles can be found in the literature with a deeper discussion and description of the state-of-the-art (Lateb et al., 2016; Tominaga and Stathopoulos, 2013, 2016; Meroney et al., 2016). However, up to the authors' knowledge, CFD has never been used before for quantitatively assessing CO_2 emissions from a power plant, and no comparisons between CFD simulations and total column measurements have been done.

Large-eddy simulations (LES) show often better agreement with experiments than using Reynolds-Averaged Navier-Stokes (RANS) equations for gas dispersion problems (Nozu and Tamura, 2012), because LES reproduces better the mean wind velocity and turbulence kinetic energy (TKE) behind the buildings if an accurate inflow turbulence (not easy task) is set (Tominaga et al., 2008). Apart from the well-known huge computational cost of LES nowadays for dealing with full-scale urban environments (Franke et al., 2007; Sumner et al., 2010), there are scientific reasons that justify the use of RANS simulations in the present investigation. Almost all the experiments used for the validation of LES simulations were carried out in wind tunnels under well-controlled and near-ideal conditions. In real atmospheric cases (i.e. in the present investigation) there is a high uncertainty due to the presence of severe disturbances (e.g. traffic, trees, very complex geometry). Such uncertainties affect both the simulation results and the experimental measurments (i.e. gas concentration and wind measurements). Patnaik et al. (2007) compared LES simulations with measurments in a real urban site, reporting some degree of reliable prediction but with a great uncertainty due to the urban environmental conditions. Therefore, we can assume that the benefits (in terms of accuracy and others) of using LES instead of RANS for simulating actual urban atmospheric environments were not scientifically demonstrated yet. We think that such comparison (LES vs. RANS for a real urban environment) has a great interest for further works, but we use only RANS in the present investigation. According to Tominaga and Stathopoulos (2016), for gas dispersion in urban environment problems where convection effects are more prominent than those of diffusion, results using steady RANS are typically acceptable when appropriate turbulence modeling is used. It is also important to mention that moving from meso-scale (WRF) to CFD (independently whether using RANS or LES) is a great improvement in terms of accuracy and attention to detail. Therefore, we identify the necessity of analyzing and improving the RANS turbulence modeling to effectively deal with this specific problem. In the present investigation we use the $k-\varepsilon$ Durbin (1996) turbulence model, especially developed for dealing with the CFD simulation of wind in urban environments.

In what follows, Section 2 comments the theory involved in fluid flow and gas dispersion and the computational modeling, Section 3 presents the simulation results compared with XCO_2 measurements on the site and with the Gaussian plume model. The optimum turbulent Schmidt number and a new parameterization for the Gaussian plume model are proposed for the urban environment. Additionally, a CO_2 concentration map for the urban area is shown. Finally, the conclusions are given in Section 4.

2. Dynamics, modeling and computational settings

2.1. Computational fluid dynamics modeling

Two steps are used for simulating the CO_2 dispersion from the power plant: the fluid flow (wind) is initially solved using the steady RANS equations, and the gas transport and diffusion is solved using the unsteady convection-diffusion equation with the wind field previously obtained. The exhaust emission from the chimney is initially considered as air for the wind flow calculation, and an exhaust composition of 13% CO_2 (Pipe Flow Calculation) is considered for solving the passive-scalar gas transport and diffusion problem. All the numerical simulations in this investigation are carried out using a self-customized version of the open-source and open-access software OpenFOAM. The advanced turbulence and gas transport modeling explained below were implemented in such a self-customized software version.

2.1.1. Governing equations for the fluid flow and turbulence modeling

Using the Reynolds decomposition, instantaneous velocity is defined as

$$u(x,y,z,t) = \overline{u}(x,y,z) + u'(x,y,z,t), \tag{1}$$

where $\overline{u}$ is the time-averaged velocity and u' denotes the fluctuating component.

The steady-state RANS equations for incompressible fluids without body forces are (Cheng et al., 2003)

$$\frac{\partial \overline{u}_i}{\partial x_i} = 0 \tag{2}$$

for mass conservation (continuity equation), and for momentum conservation

$$\frac{\partial\left(\overline{u}_i\overline{u}_j\right)}{\partial x_j} = -\frac{1}{\rho}\frac{\partial \overline{p}}{\partial x_i} + \frac{\partial}{\partial x_j}\left(\nu\frac{\partial \overline{u}_i}{\partial x_j} - \overline{u_i'u_j'}\right), \tag{3}$$

where $\overline{p}$ is the mean pressure, ρ the fluid density, ν the kinematic viscosity and $\overline{u_i'u_j'}$ are Reynolds stresses that can be computed from the mean flow values (statistical turbulence closure). Considering the Boussinesq linear isotropic eddy-viscosity hypothesis, which assumes a linear relationship between turbulent stresses and mean velocity gradients, it yields

$$-\overline{u_i'u_j'} = 2\nu_t S_{ij} - \frac{2}{3}k\delta_{ij}, \tag{4}$$

where S_{ij} is the strain rate tensor, ν_t the kinematic eddy viscosity, δ_{ij} the Kronecker Delta function and $k = \frac{1}{2}\overline{u_i'u_i'}$ is the turbulent kinetic energy. Two additional equations for turbulence kinetic energy (k) and turbulence dissipation (ε) are necessary in order to solve all the unknowns of the problem. These equations (steady-state without buoyancy) are

$$\frac{\partial(\overline{u}_j k)}{\partial x_j} = \frac{\partial}{\partial x_j}\left[\left(\nu + \frac{\nu_t}{\sigma_k}\right)\frac{\partial k}{\partial x_j}\right] + P_k - \varepsilon \tag{5}$$

and

$$\frac{\partial(\overline{u}_j \varepsilon)}{\partial x_j} = \frac{\partial}{\partial x_j}\left[\left(\nu + \frac{\nu_t}{\sigma_\varepsilon}\right)\frac{\partial \varepsilon}{\partial x_j}\right] + C_{\varepsilon 1}\frac{\varepsilon}{k}P_k - C_{\varepsilon 2}\frac{\varepsilon^2}{k}, \tag{6}$$

where P_k is the production of k. σ_k and σ_ε (Prandtl numbers), $C_{\varepsilon 1}$ and $C_{\varepsilon 2}$ are closure constants. The production of k in the standard $k-\varepsilon$ model (SKE) is computed as

$$P_k = \nu_t S^2, \tag{7}$$

where S is the modulus of the rate of strain tensor.

Notice that we neither consider buoyancy nor use the energy equation, therefore we neglect the effect of the exhaust temperature (around 90 °C). Apart from that the difference in the air density between exhaust and environment is not very significant, we can assume that momentum is dominant on the flow because a downwash effect takes place, which is given by the low speed of the exhaust, lower than 1.5 times the wind speed at chimneys height. This is, low pressure in the wake of the chimney causes the plume to be downward behind the chimney. This effect is augmented by the large dimensions of the power plant building, and by the presence of surrounding buildings. A deeper explanation of the downwash effect can be found in Hanna et al. (1982).

There are some modifications of the SKE model (e.g. Launder and Kato (1993), Murakami-Mochida-Kondo (Tsuchiya et al., 1997), Yap (1987)), developed to improve the accuracy of the results, especially the overestimation of the turbulent kinetic energy in the impinging region of bluff bodies. Durbin (1996) proposed a $k-\varepsilon$ modification by calculating ν_t related to the turbulence velocity time scale (T),

$$\nu_t = C_\mu k T, \tag{8}$$

where C_μ is the proportional number, another constant parameter. The proposed bound on the time scale of Durbin (1996) is

$$T = \min(T_{SKE}, T_D), \tag{9}$$

where

$$T_{SKE} = k/\varepsilon \tag{10}$$

and

$$T_D = \frac{1}{3C_\mu S}\sqrt{\frac{3}{2}}. \tag{11}$$

The Durbin (1996) turbulence model is used in the CFD simulations for the present investigation. The coefficients used in the equations are $C_\mu = 0.09$, $C_{\varepsilon 1} = 1.44$, $C_{\varepsilon 2} = 1.92$, $\sigma_k = 1.0$, $\sigma_\varepsilon = 1.3$ and $\kappa = 0.4$. We have already successfully validated this turbulence modeling setting in Toja-Silva et al. (2015a) by studying the benchmark case A of the Architectural Institute of Japan (Yoshie et al., 2007; Architectural Institute Japan (AIJ), 2016; Guidebook for practical applications of CFD to pedestrian wind environment around buildings). This benchmark case is an isolated building of aspect ratio 1:1:2 placed within an atmospheric boundary layer inside a wind tunnel, tested by Meng and Hibi (1998). Hit rates of $HR_U = 87.5\%$ and $HR_k = 75.0\%$ have been obtained (Toja-Silva et al., 2015a).

2.1.2. Gas transport and diffusion modeling

As stated above, since the total chimney exhaust is computed as air in the fluid flow calculation, the CO_2 emission can be considered as a passive scalar in the gas transport and diffusion calculation, assuming that the chimneys exhaust is 13% CO_2. The gas transport and diffusion problem is solved using the convection-diffusion passive scalar equation for incompressible turbulent flows (Shen et al., 2002):

$$\frac{\partial C}{\partial t} + \frac{\partial\left(\overline{u}_j C\right)}{\partial x_j} - \frac{\partial}{\partial x_j}\left(D_{eff}\frac{\partial C}{\partial x_j}\right) = 0, \tag{12}$$

where C is the averaged volumetric CO_2 concentration in parts per million (ppm) and $D_{eff} = D + D_t$ is the effective diffusivity. The molecular diffusivity used is $D = 1.6 \cdot 10^{-5}$ m^2 s^{-1} (Lide, 2004), and the eddy diffusivity is computed as

$$D_t = \frac{\nu_t}{Sc_t}, \tag{13}$$

where Sc_t corresponds to the turbulent Schmidt number. According to Tominaga and Stathopoulos (2007), the optimum values for Sc_t are widely distributed in the range $0.2 - 1.3$ and the selected value has a big impact on the results. The selection of the appropriate value depends on the characteristics of the flow, being recommended $Sc_t = 1$ for a plume dispersion in an atmospheric boundary layer (Tang et al., 2006). Therefore, $Sc_t = 1$ is used in the present investigation for the open field case. For the urban environment case, different values of the turbulent Schmidt number ($Sc_t = 0.4 - 1.2$) are tested. We suggest the most suited value of the turbulent Schmidt number for being used in full-scale simulations, according to the best agreement with the experimental results.

2.1.3. Boundary conditions

Table 1 shows the boundary conditions imposed in the simulations. Since $30 < y^+ < 1000$, standard turbulent wall laws (Blocken et al., 2007; Parente et al., 2011; O'Sullivan et al., 2011) can be used for the treatment of the near wall flow. For the ground, sand-grain-based fully rough law of the wall is used. The equivalent sand-grain roughness height is calculated as (Blocken et al., 2007):

$$k_s = \frac{9.793 z_0}{C_s}, \tag{14}$$

where z_0 is the aerodynamic roughness length and $C_s = 7$ (van Hooff and Blocken, 2010) is the roughness constant.

The inlet wind profiles used are computed according to Richards and Hoxey (1993), using

$$U = \frac{U_*}{\kappa}\ln\left(\frac{z + z_0}{z_0}\right), \tag{15}$$

$$k = \frac{U_*^2}{\sqrt{C_\mu}} \tag{16}$$

and

$$\varepsilon = \frac{U_*^3}{\kappa(z + z_0)}, \tag{17}$$

Table 1
Boundary conditions imposed at each boundary of the domain. Nomenclature: *Cc* = Calculated, fV = fixedValue, iV = inlet value, sl = slip, wF = wall function, zG = zeroGradient.

	U	k	ε	ν_t	p	C
Inlet	iV	iV	iV	*Cc*	zG	iV
Outlet	zG	zG	zG	*Cc*	fV zero	zG
Ground	fV zero	kqR wF	epsilon wF	nutk rough wF	zG	zG
Buildings	fV zero	kqR wF	epsilon wF	nutk wF	zG	zG
Chimneys	iV	iV	iV	*Cc*	zG	iV
Sky	sl	sl	sl	*Cc*	zG	zG
Sides	sl	sl	sl	sl	sl	zG

where $z_0 = 0.2$ m. Using Eq. (15), U_* is calculated for each case considering the reference values $z_{ref} = 30$ m (height of wind measurement) and U_{ref} (wind speed at the simulated moment). Although it is a common practice in CFD, we do not use in this article dimensionless magnitudes (with respect to these reference values) because, on the one hand, the results may be different than considering reduced scales, e.g. wind tunnel where the Reynolds number is some orders of magnitude lower (Toja-Silva et al., 2015b), and on the other hand, this work is oriented to further atmospheric environmental applications, where real magnitudes are always presented.

2.1.4. Computational settings

The simpleFoam solver for steady-state incompressible turbulent flows is used for solving the fluid flow governing partial differential equations in OpenFOAM. For the gas transport and diffusion problem, the customized solver turbulentScalarTransportFoam (that has the structure of the original solver scalarTransportFoam) is employed to solve the convection-diffusion passive scalar equation including the turbulent eddy dissipation. The simulations are carried out on 84 parallel processors in a cluster (Linux Cluster).

Gaussian integration with different interpolation schemes is adopted

(a) Location of the area of study in Munich (Germany)

(b) Detail view area of study

Fig. 1. General view of the area of study (adapted from Google Maps).

for the spatial discretization of differential operators. Second order linear interpolation is applied for Gradient terms and divergences, and 2nd order linear interpolation with explicit non-orthogonal correction is used for Laplacian terms. With respect to the linear system solvers, generalised geometric-algebraic multi-grid solver (GAMG) with DIC smoother is used for pressure, and preconditioned bi-conjugate gradient solver for asymmetric matrices (PBiCG) with diagonal incomplete LU (DILU) preconditioner is used for the rest of the variables.

Convergence criteria are set to at least 10^{-5} for all the residuals, a value very frequently reported in the literature (Jeanjean et al., 2015; Ferziger and Perić, 2002). Although 10^{-3} is commonly used for industrial applications (Franke et al., 2007), values below 10^{-4} are recommended in order to obtain a converged solution (Takano and Moonen, 2013). However, monitoring the evolution of the residuals is always necessary. For the convection-diffusion equation (i.e. gas dispersion problem), we reach residual values below 10^{-6} in order to ensure the solution stabilization. Additionally, it is necessary to analyze the results looking for possible undesired oscillations and/or divergences that may require special attention. In order to avoid such instabilities, we use a relaxation factor of 0.3 for pressure and high quality initial conditions, i.e. results from precursor simulations using 1st order numerical schemes (more stable but less accurate).

Regarding the meshing, a background mesh is constructed using the structured blockMesh application and the geometry (power plant and buildings), previously designed with a CAD tool and saved in STL format, is embedded into the background mesh using the snappyHexMesh application of OpenFOAM (SnappyHexMesh). The mesh is refined around the buildings and adapted to their shape. The refinement distance is 40 m around the power plant and 10 m around the rest of the buildings.

2.2. The Gaussian plume model

Under certain idealized conditions, the mean concentration of a species emitted from a point source has a Gaussian spatial distribution (Seinfeld and Pandis, 2006). The general expression of the Gaussian plume model for a contaminant concentration c (mass per unit volume) at a point (x, y, z) downstream of the emission source $(x = y = 0, z = h_{ch})$ is (Seinfeld and Pandis, 2006; Reynolds, 1992)

$$c = \frac{Q}{2\pi\sigma_y\sigma_z U_{ch}} \exp\left(-\frac{y^2}{2\sigma_y^2}\right)\left[\exp\left(-\frac{(z-h_{ch})^2}{2\sigma_z^2}\right) + \exp\left(-\frac{(z+h_{ch})^2}{2\sigma_z^2}\right)\right], \tag{18}$$

where Q is the mass of material released per unit time, h_{ch} is the emission source (chimneys) height, U_{ch} is the free-stream wind speed at the chimneys height, and $\sigma_y(x)$ and $\sigma_z(x)$ are standard deviation in cross-wind and vertical directions (dispersion parameters), respectively. For a neutrally stratified atmosphere (condition assumed for the simulations), these dispersion parameters can be computed as (Briggs, 1973)

$$\sigma_y = 0.08x(1 + 0.0001x)^{-\frac{1}{2}} \tag{19}$$

and

$$\sigma_z = 0.06x(1 + 0.0015x)^{-\frac{1}{2}}. \tag{20}$$

Briggs (1973) also suggests a specific vertical dispersion parameter for an urban environment,

$$\sigma_z = 0.14x(1 + 0.0003x)^{-\frac{1}{2}}. \tag{21}$$

These are the parameters recommended by the ALOHA Review Committee (Reynolds, 1992). Although the Gaussian plume equation is applied widely (Environmental Protection Agency, 1980), the conditions under which the Gaussian equation is valid are highly idealized (i.e. stationary and homogeneous turbulence) and it is not applicable to every actual ambient situation. For valid applications, the dispersion parameters (σ_y and σ_z) have to be derived from actual atmospheric diffusion experiments under conditions approximating those of the application

Fig. 3. View of one of the spectrometers used for obtaining the measurement data used in this investigation.

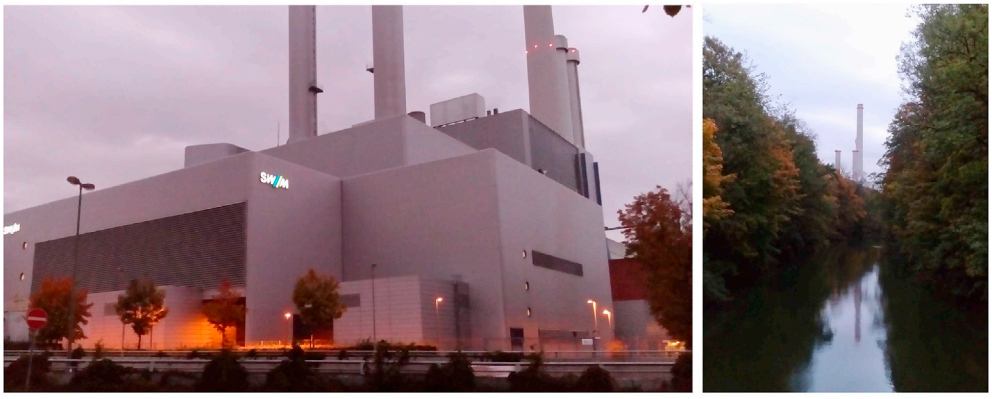

(a) External view of the building (b) View of the chimneys from far away

Fig. 2. Views of the power plant from the south.

Table 2
Case studies selected for the investigation.

Name of the case study	U_{ref}	Incident wind direction
Open field	2.4 m s^{-1}	354°(NWN)
Urban environment	1.38 m s^{-1}	67.5°(ENE)

(Seinfeld and Pandis, 2006). Therefore, an accurate parametrization of the Gaussian plume model for urban environments is needed. Such parametrization must be derived from a well controlled case study as in the present investigation: numerical simulation (using accurately validated turbulence modeling) compared with actual experimental measurements.

3. CFD simulation and XCO_2 measurement in a real urban site

3.1. General description of the problem

The area of study is in Sendling, inside the city of Munich (Germany),

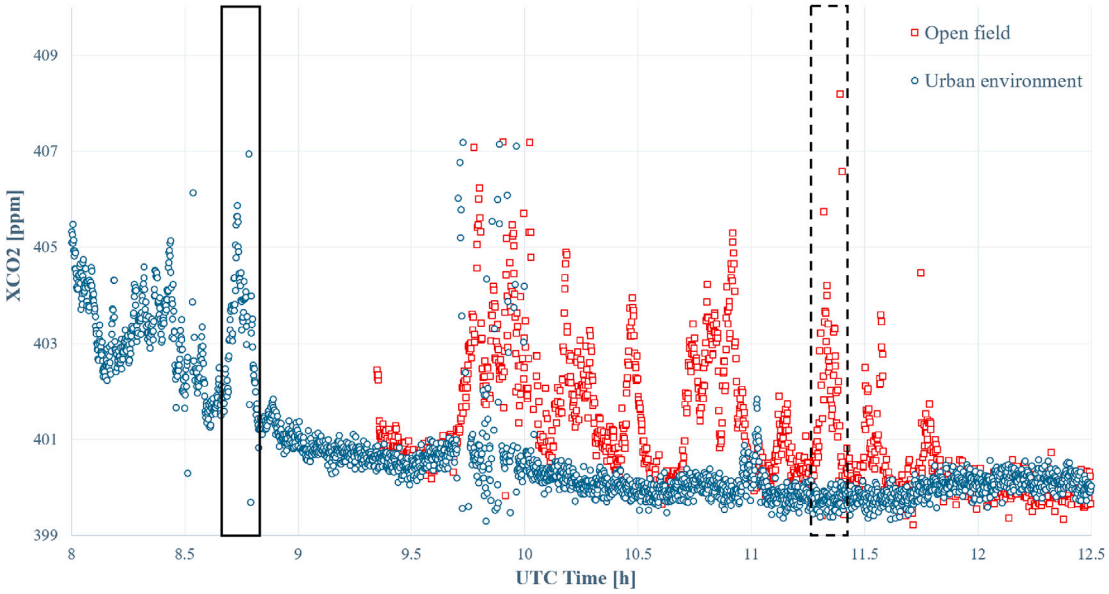

Fig. 4. XCO_2 values measured during the target day. Solid square: urban environment case. Dashed square: open field case.

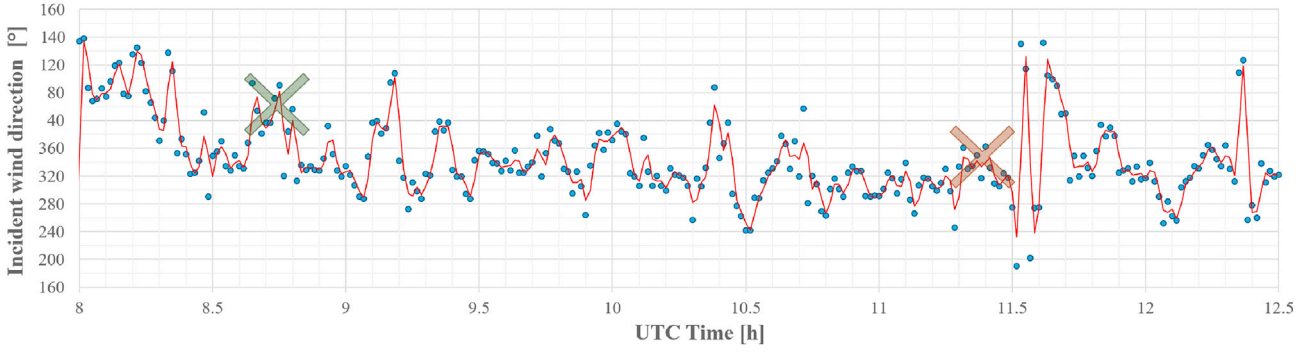

(a) Wind direction (0°≡ 360°≡ wind from the Nord)

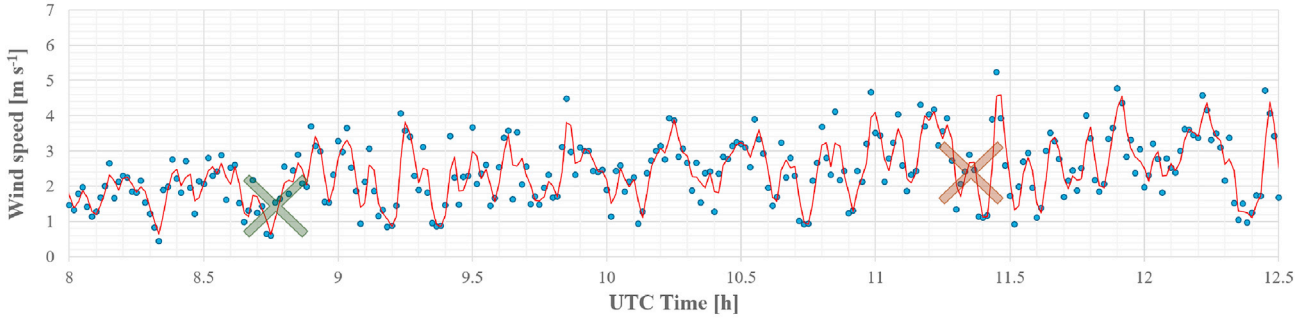

(b) Wind speed

Fig. 5. Wind direction and speed at 30 m height during the target day. Green cross: urban environment case. Red cross: open field case. Blue dots: experimental values. Red line: average trendline. (For interpretation of the references to colour in this figure legend, the reader is referred to the web version of this article.)

around 4 km from the city center in SW direction. Fig. 1 shows a general view of the area and the most important sites: the power plant and the two measurement points. Both measurement sites are placed at a distance of around 0.5 km from the power plant in SES (open field) and WSW (urban environment), respectively.

In what follows, two simulations are carried out, one corresponding to each measurement site. Firstly, the wind measurements were analyzed in order to find an instant when the measurement point was placed exactly downstream from the power plant (NWN and ENE wind directions, respectively). According to the information kindly provided by the responsible company Stadtwerke München GmbH (SWM), this power plant has a total maximum power of 1512 MW: 698 MW of electrical power and 814 MW of thermal energy generation. The instantaneous natural gas fuel consumption at the measurement time was also kindly provided by SWM, allowing us to accurately compute the emission from each chimney. Fig. 2 shows the power plant building and a view of the chimneys from far away. It has 5 chimneys: the central chimney (highest) has no GHG emissions, the 2 chimneys at the north have a height of 130 m, and the 2 chimneys at the south have a height of 90 m.

3.2. XCO_2 and wind measurements

We deployed two Bruker EM27SUN (Gisi et al., 2012; Frey et al., 2015) compact Fourier transform spectrometers to make simultaneous measurements of column amounts of CO_2 using the sun as the light source. The spectrometers measure the column number densities (total column) of CO_2 and O_2, the ratio of which gives the column-averaged dry-air mole franction of CO_2 (XCO_2). The spectrometer EM27SUN has higher precision in retrieving XCO_2 (Gisi et al., 2012; Chen et al., 2016; Hedelius et al., 2016) compared to the Bruker IFS 125HR, which is used

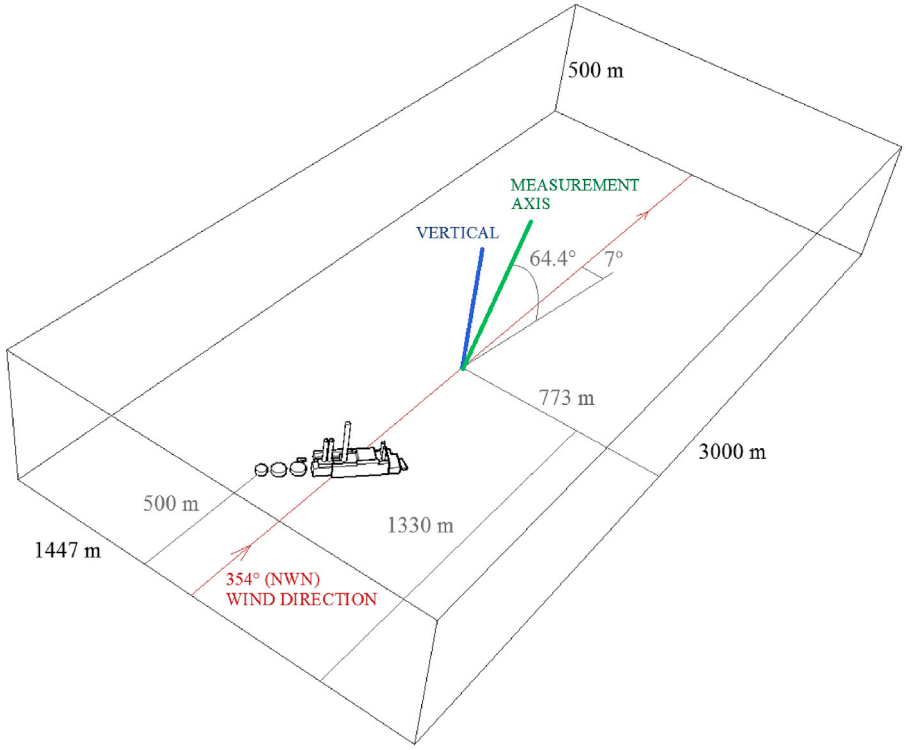

(a) Details of the domain and the XCO_2 measurement axis

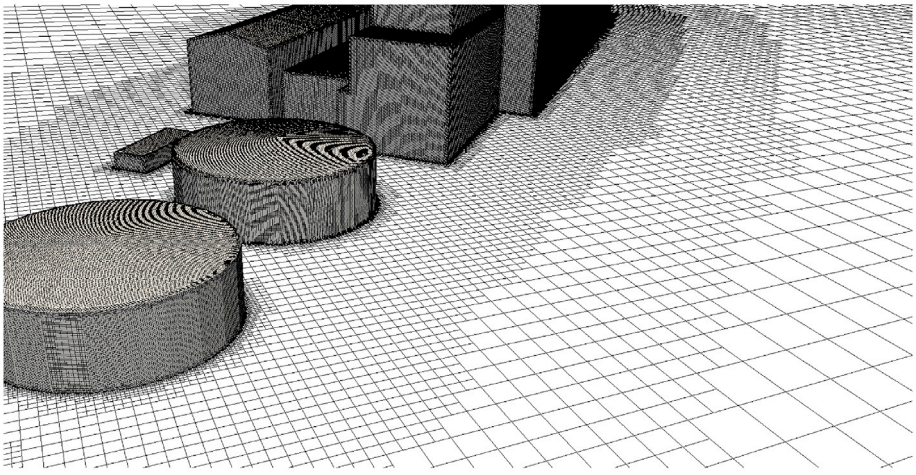

(b) Mesh of the domain, 8.3 M cells

Fig. 6. Geometry of the open field case study: incident wind 354°(NWN).

in the total carbon column observing network (TCCON) (Wunch et al., 2011). According to the Allan analysis (Chen et al., 2016), the precision of the differential column measurement is 0.04 ppm with 10 min integrating time, around 0.12 ppm when averaging over 1 min, and near 0.4 ppm for one single measurement. In general, the precision decreases proportionally to the square root of integration time (≤10 min). The performance is very stable after relocation across country and continent (Frey et al., 2015; Chen et al., 2016). Fig. 3 shows one of the spectrometers used for obtaining the measurement data used in this investigation. They are compact and autonomous, and thus adequate for portable applications, as in the present case.

The XCO_2 measurement corresponds to the averaged concentration of CO_2 in the slant column. Therefore, the concentration profiles obtained using both CFD simulations and the Gaussian plume model will be averaged in the whole troposphere (i.e. 12,000 m height) considering a homogeneous background concentration, in order to be compared with XCO_2 measurements. According to that, it is noticed that the geometry of the problem has a great relevance, because the XCO_2 value has a strong dependency on how the measurement axis crosses the plume. It makes the comparison challenging and it can be the reason why, up to the authors' knowledge, there are no previous comparisons between CFD

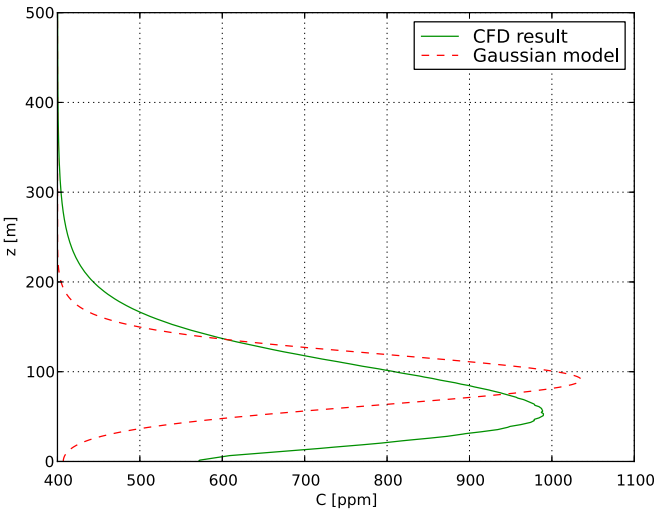

Fig. 8. Comparison between XCO_2 simulation results and the Gaussian plume model on the measurement point for the open field case.

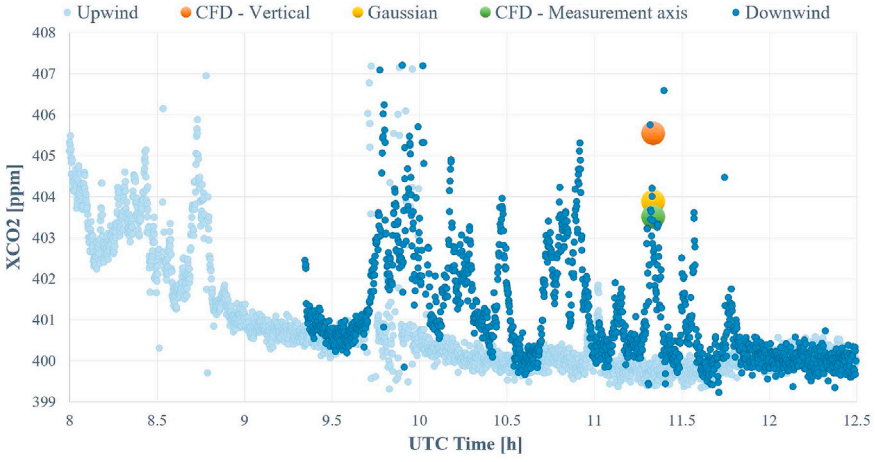

(a) Comparison between simulation and experimental results

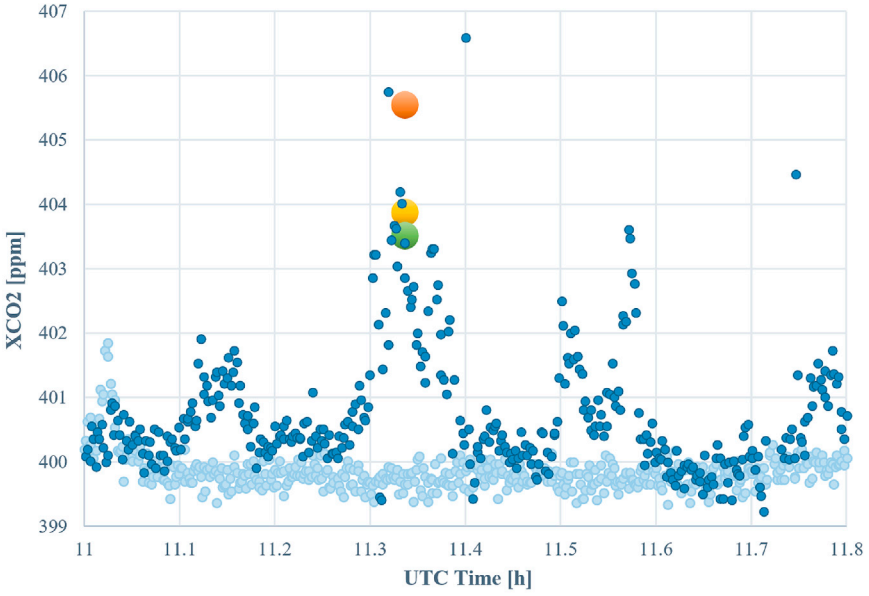

(b) Zoom around the time of interest

Fig. 7. Quantitative results for XCO_2 for the open field case.

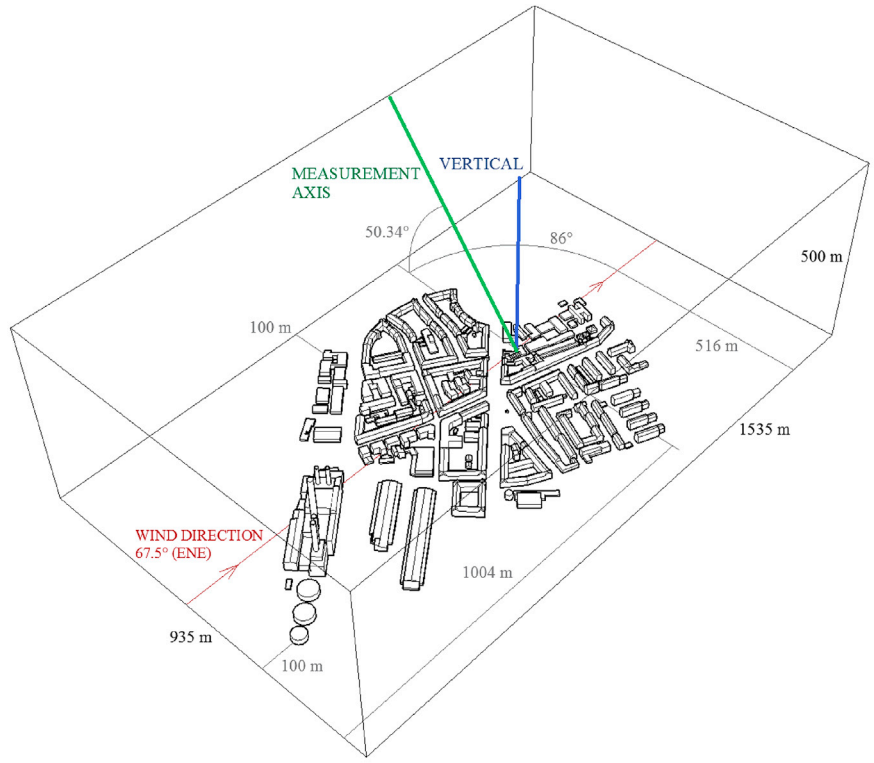

(a) Details of the domain and the XCO_2 measurement axis

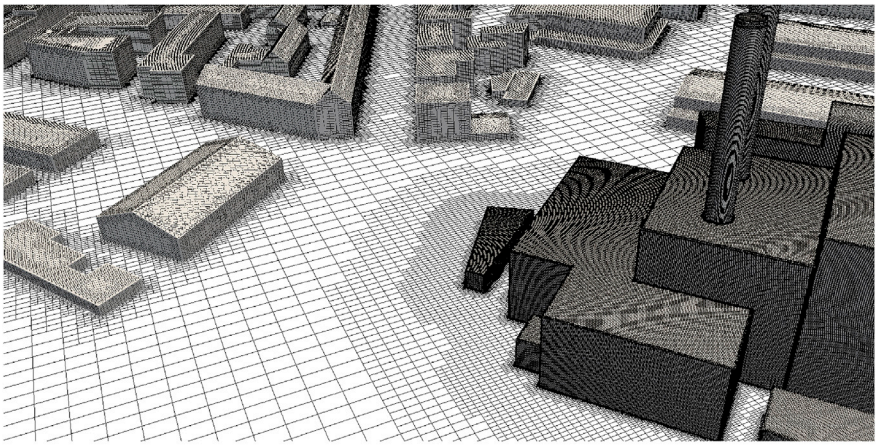

(b) Mesh of the domain, 18.7 M cells

Fig. 9. Geometry of the urban case study: incident wind 67.5°(ENE).

simulation results and column measurements in the literature.

The case studies simulated are chosen according to two criteria: observing peaks in the XCO_2 measurement and having the measurement sites downstream of the emission source (power plant) simultaneously. Table 2 shows the two case studies selected according to these criteria in order to analyze the experimental results obtained at the two measurement sites. Fig. 4 shows the XCO_2 values measured in both sites, and Fig. 5 shows the wind speed and direction during the target day. The selected moments (case studies) are also represented in Figs. 4 and 5. The wind measurements used in this investigation were taken on the roof of the Ludwig-Maximilians-Universität München ($z_{ref} = 30$ m), 4.5 km north from the power plant. We focus in the present investigation on the two cases of study that satisfy the criteria explained above. The usage of the whole dataset presented in Fig. 4 for emission estimation (including discussion on measurement strategies) is presented in Chen et al. (2017).

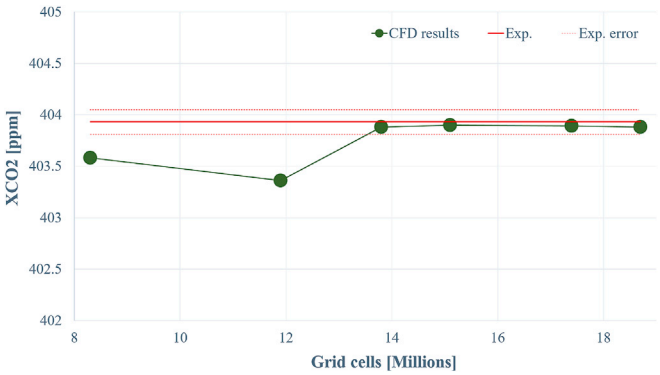

Fig. 10. Comparison between XCO_2 simulation results using 6 different mesh sizes.

3.3. Open field - wind 2.4 m/s and 354° (NWN)

3.3.1. Description of the case

The first case study presented occurs in an open field. Fig. 6 shows the geometry (only the power plant) and the resulting mesh. A long distance is set downstream in order to verify the plume and to compare it with the Gaussian model. The surrounding distances recommended in the Best Practice Guidelines (Franke et al., 2007) are respected.

This wind condition ($U_{ref} = 2.4$ m s^{-1} and incident direction 354°, NWN) was chosen attending to the two criteria mentioned above: simultaneously observing peaks in the XCO_2 measurements and having the measurement site downstream of the power plant. According to the CH_4 consumption rate reported by SWM, the total emission during the study time is 43.3 kgCO_2 s^{-1}. Considering chimneys geometry and the emission from each chimney, the exhaust speed is set to $U_{ch,N} = 0.5$ m s^{-1} and $U_{ch,S} = 2.0$ m s^{-1} for North and South chimneys, respectively. The CO_2 content in the exhaust is set to 13% for all the chimneys, and the CO_2 concentration in the environment is 400 ppm. As stated above, $Sc_t = 1$ is used for this case study.

3.3.2. Results and discussion

The experimental value obtained at the case study time shows a high variability in the range 402.85 − 404.2 ppm (mean 403.53 ppm). This high variability is due to the high variability of the wind conditions (both speed and direction), as is shown in Fig. 5.

Fig. 7 shows the simulation results obtained for the open field case. A comparison of the XCO_2 simulation results with the experimental values is presented. The XCO_2 was calculated from the simulation results both considering a vertical column and on the real axis of measurement, using the instantaneous azimuth and elevation angles from the experiment. The XCO_2 simulation results are 405.55 ppm, 403.89 ppm and 403.52 ppm for CFD vertical column, Gaussian model and CFD on measurement axis, respectively. The results show a reasonably good agreement between simulation and experimental results. The XCO_2 value calculated considering the measurement axis angle shows the best agreement with the mean experimental result, yielding absolute and relative errors of −0.01 ppm and 0.002%, respectively. This error is one order of magnitude lower than the measurement error. It is observed that the consideration of both azimuth and elevation angles has a strong impact on the results. However, since the measurement axis is rather aligned with the streamwise direction, the results obtained using the Gaussian plume model show also a good agreement, although they are computed considering a vertical column. Additionally, it is observed in the measurements that the downwind values show some peaks (e.g. at the case study time) and fall down to the upwind range. Therefore, we can also esitmate the background CO_2 concentration using only the downwind data.

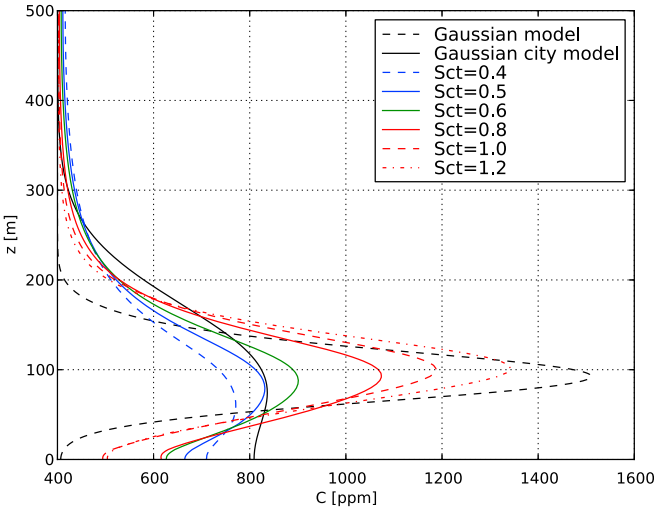

Fig. 12. Urban case comparison of vertical profiles obtained from simulations using different Sc_t numbers and using the Gaussian plume model (with standard deviation coefficients suggested in the literature for both open fields and urban environments).

Fig. 8 shows a comparison of the vertical section on the measurement point between the results obtained with the CFD simulation and the result of calculating the plume using the Gaussian model. The results show a reasonably good agreement. Although this is an open field case, the effect of the turbulence induced by the power plant building is observed in the simulation results. Such effect results in an enhancement of the turbulent eddy dissipation near the ground, reflected in both a lower height for the peak values and the wider shape of the concentration profile obtained in the CFD simulations compared with the Gaussian plume model.

3.4. Urban environment - wind 1.38 m/s and 67.5° (ENE)

3.4.1. Description of the case

The second case study is the core of this investigation, and focuses on a residential urban area. Fig. 9 shows the geometry and the resulting

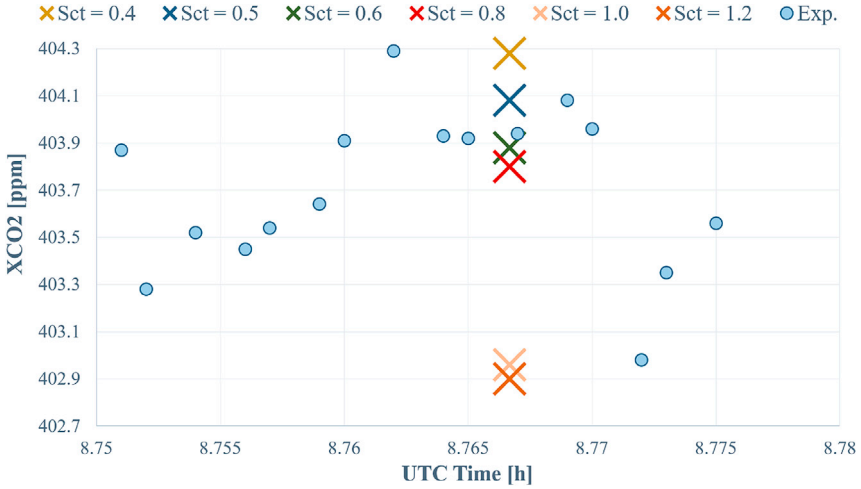

Fig. 11. Comparison for the urban case of XCO_2 simulation results using different Sc_t numbers on the real axis of measurement.

mesh. The domain size is defined according to the Best Practice Guidelines (Franke et al., 2007).

As in the previous case, the wind condition ($U_{ref} = 1.38$ m s^{-1} and incident direction 67.5°, ENE) was chosen attending to the observation of peaks in the XCO_2 measurements while the measurement site is located downstream from the power plant. According to SWM, the power plant operated with the same power load during both case studies (total emission 43.3 kgCO_2 s^{-1}) and, therefore, the exhaust speed is also set to $U_{ch,N} = 0.5$ m s^{-1} and $U_{ch,S} = 2.0$ m s^{-1} for North and South chimneys, respectively. The CO_2 content in the exhaust is again set to 13% for all the chimneys. As observed in the open field case study, the measurements at the downwind site show peak values (i.e. at the case study time) and fall down to the upwind range and, therefore, it is suggested that it is possible to estimate the environment CO_2 concentration looking at this lower background range at the same downwind data. Since no upwind data is available for the urban environment case study, a CO_2 concentration in the environment of 401.4 ppm is determined using that method. This background CO_2 can be clearly observed in Fig. 13b. In this case study, different values of the turbulent Schmidt number are tested and the most suited for being used in full-scale urban dispersion simulations is proposed.

3.4.2. Mesh sensitivity analysis

Fig. 10 shows a comparison of the simulation results obtained for XCO_2 using 6 different mesh sizes: 8.3M, 11.9M, 13.8M, 15.1M, 17.4M and 18.7M cells, respectively. Due to the extreme complexity of the geometry, a convergence tendency is not observed for the coarse meshes, i.e. the coarsest mesh occasionally gave a better result than with 11.9M cells. However, convergence is clearly observed for $\geq$13.8M cells. Since the configuration corresponding to the finest mesh (18.7M cells) is used in all the computations presented in this article, the mesh independence of the results is guaranteed.

3.4.3. The influence of the turbulent Schmidt number on the gas dispersion

In this case study, the experimental values are rather constant in the range 403.92 – 403.94 ppm. This is because the wind (both speed and direction) is more stable than in the open field case.

As stated above, the turbulent Schmidt number has a strong influence

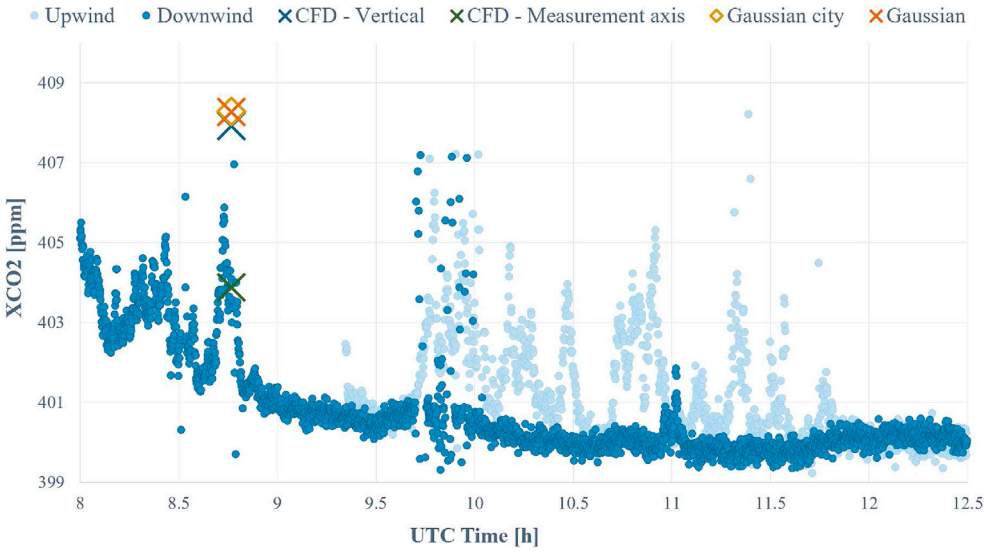

(a) Comparison between simulation and experimental results

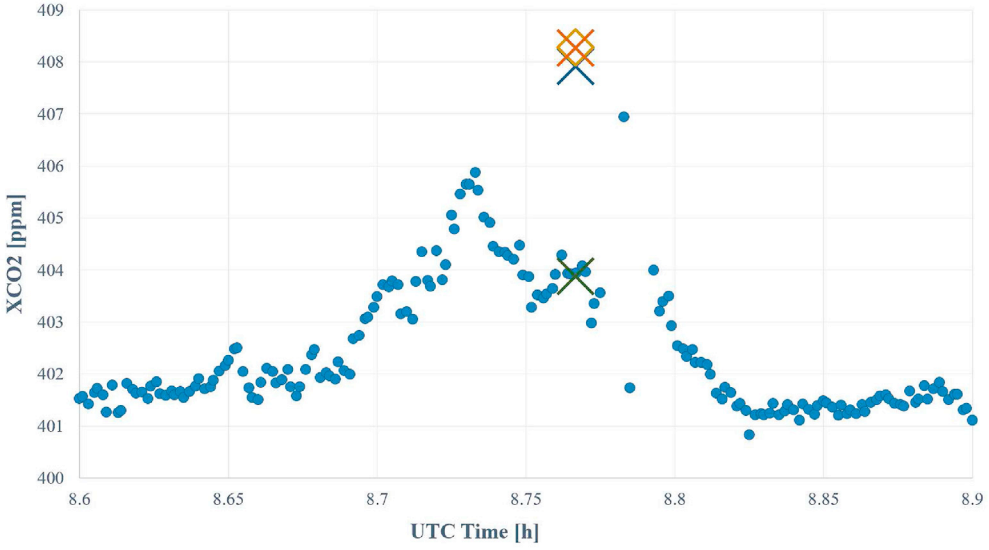

(b) Zoom around the time of interest

Fig. 13. Quantitative results for XCO_2 for the urban environment case.

on the results. Fig. 11 shows a comparison of experimental and simulation values of XCO_2 using different turbulent Schmidt numbers ($Sc_t = 0.4 - 1.2$) on the real axis of measurement, using azimuth and elevation angles from the experiment at the moment considered. It is observed that Sc_t values in the range of $Sc_t = 0.5 - 0.8$ present a very good agreement with the experimental results. The best agreement is found for $Sc_t = 0.6$, with a XCO_2 value of 403.88 ppm. The absolute and relative deviations between experimental and simulation results are −0.05 ppm and 0.01%, respectively. This error is one order of magnitude lower than the measurement error. Therefore, according to our results, we suggest this value for being used in further full-scale urban dispersion simulations. Turbulent kinetic energy (TKE) in the urban environment is underestimated in the simulations because aspects such as traffic are not taken into account. Lower values of the turbulent Schmidt number (i.e. $Sc_t = 0.6$) compensate such underestimation of TKE when computing the turbulent eddy dissipation in the gas transport and diffusion equation. This value is in agreement with other researchers, as Gromke and Blocken (2015) that suggest $Sc_t = 0.5$ for gas dispersion in a street canyon with trees. In our investigation, the value is slightly higher because we are considering the whole urban area (streets with and without trees), and also above the buildings.

Fig. 12 shows a comparison of the vertical section on the measurement point between the results obtained from the CFD simulations using different Sc_t numbers and the result of calculating the plume using the Gaussian model, considering standard deviation coefficients suggested in the literature for both open fields and urban environments. As expected, a strong influence of the turbulent eddy dissipation phenomena that enhance the gas diffusion close to the buildings is observed. This effect cause a wider shape of the concentration profile, and a decrease of peak values. It is also observed that the simulation results using $Sc_t = 0.6$ (and using low Sc_t values in general) show a profile more similar to the Gaussian model using the urban parametrization than using the standard parametrization used for open field cases. However, there is still a necessity of improving the Gaussian plume model suggested for urban environments, i.e. the black line should be more similar to the green line in Fig. 12. Therefore, a better parametrization for the Gaussian model is proposed below.

3.4.4. *Results using $Sc_t = 0.6$*

Fig. 13 shows a comparison of the XCO_2 simulation results using $Sc_t = 0.6$ with the experimental values for the urban environment case. The XCO_2 was calculated from the simulation results, both considering a

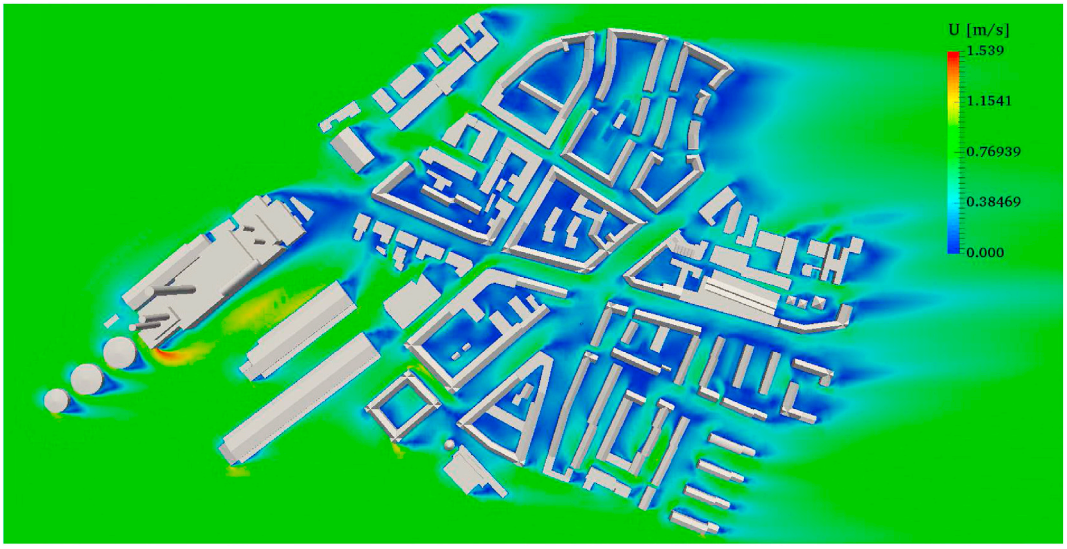

(a) Horizontal slice of velocity at $z = 4$m

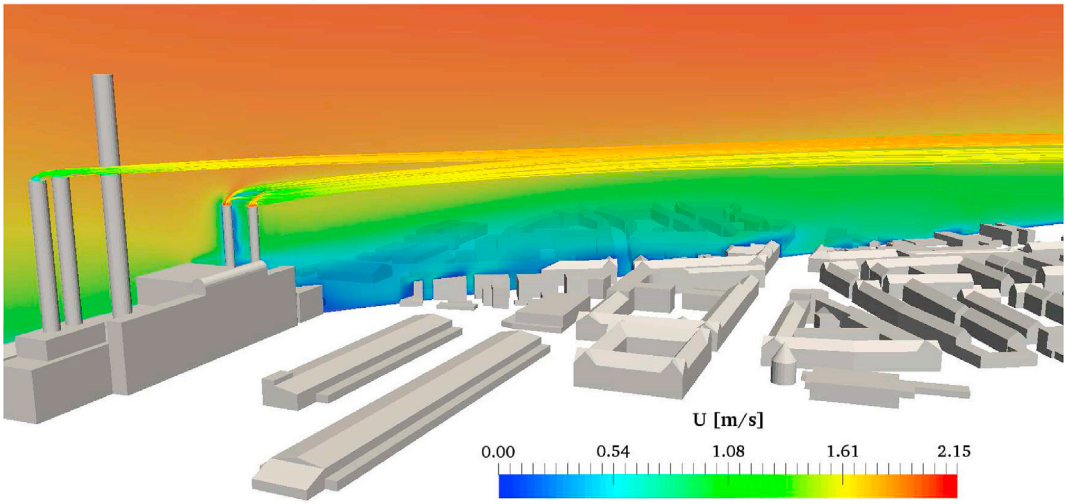

(b) Vertical slice of velocity and streamlines

Fig. 14. Images of the wind velocity for the urban environment case.

vertical column and on the real axis of measurement. The results confirm that both azimuth and elevation angles have to be taken into account for designing measurement campaigns, because the XCO_2 values expected for the vertical column are clearly higher than those obtained at the experiment, and they show good agreement when the measurement axis angles are taken into account, as in the open field case.

Fig. 14 shows images of the wind velocity for the urban environment case. It is observed that wind velocity dramatically decreases in the urban environment due to the obstacles. However, an acceleration effect is observed in transversal street canyons and open spaces around big structures (e.g. behind the power plant building). Specifically, the power plant has a significant effect on the surroundings due to its big dimensions, causing a high acceleration of the wind around the corners. Additionally, the streamlines of the exhaust show that the height of the plume keeps rather constant at the chimneys height, specially for the highest chimneys because the exhaust mass flow is lower and, therefore, the exhaust velocity is also lower.

Fig. 15 shows images of turbulent kinetic energy for the urban environment case. It is observed that TKE has a high value above the buildings, which induces a high diffusion effect on this region compared to the open field case. Of course, high values of TKE are observed around the chimney walls. Additionally, high values of TKE are shown at the ground level around the highest buildings, and when a building wake affects another building (e.g. downstream of the power plant).

Fig. 16 shows vertical and horizontal maps of the CO_2 concentration in the urban area. Both transport and diffusion are observed in the maps. Due to the diffusion phenomenon caused by the turbulent eddy dissipation, the gas concentration tends to be higher at the ground level than above 100 m (where the diffusion is smoother). It is shown that the plume even changes the trajectory for approaching to the ground at a distance of around 500 m. Slightly further away, at around 700 m downstream from the power plant, high concentrations ($\geq$ 700 ppm) of CO_2 are observed at the ground level. Therefore, having punctual ground measurements of CO_2 concentration in this area will be of great interest in further investigations.

Fig. 17 shows isosurfaces of the CO_2 concentration. A strong convective effect is observed inside the street canyons, because the gas concentration is lower when the wind comes from outside the gas cloud (upstream effect) and it is higher when the wind comes from inside the gas cloud (downstream effect). This downstream effect is clearly

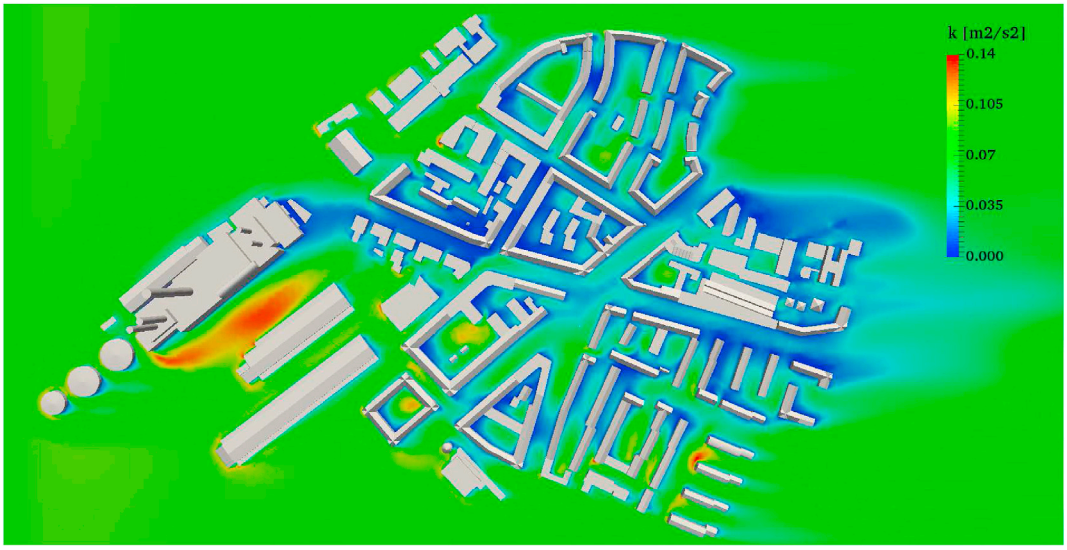

(a) Horizontal slice of k at $z = 4$m

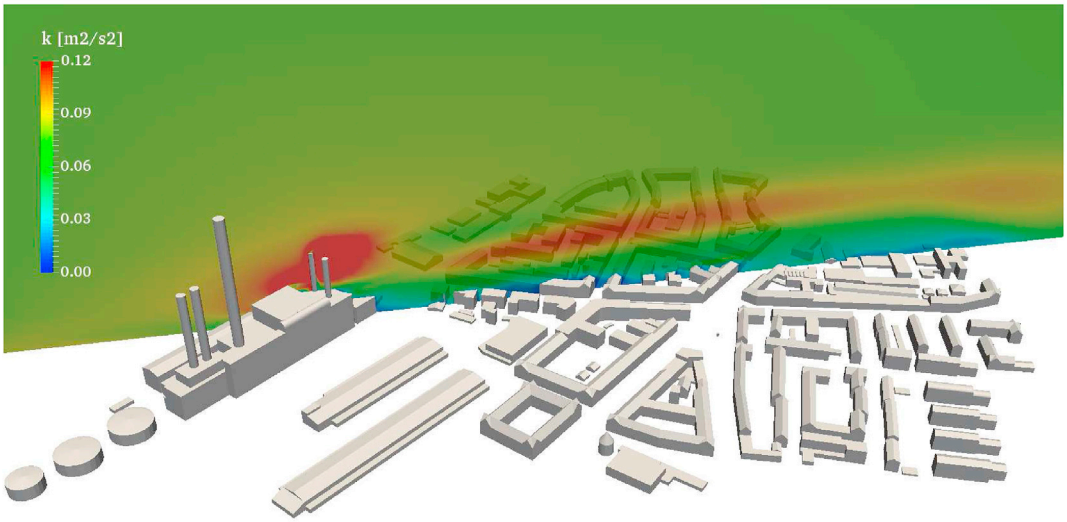

(b) Vertical slice of k

Fig. 15. Images of turbulent kinetic energy for the urban environment case.

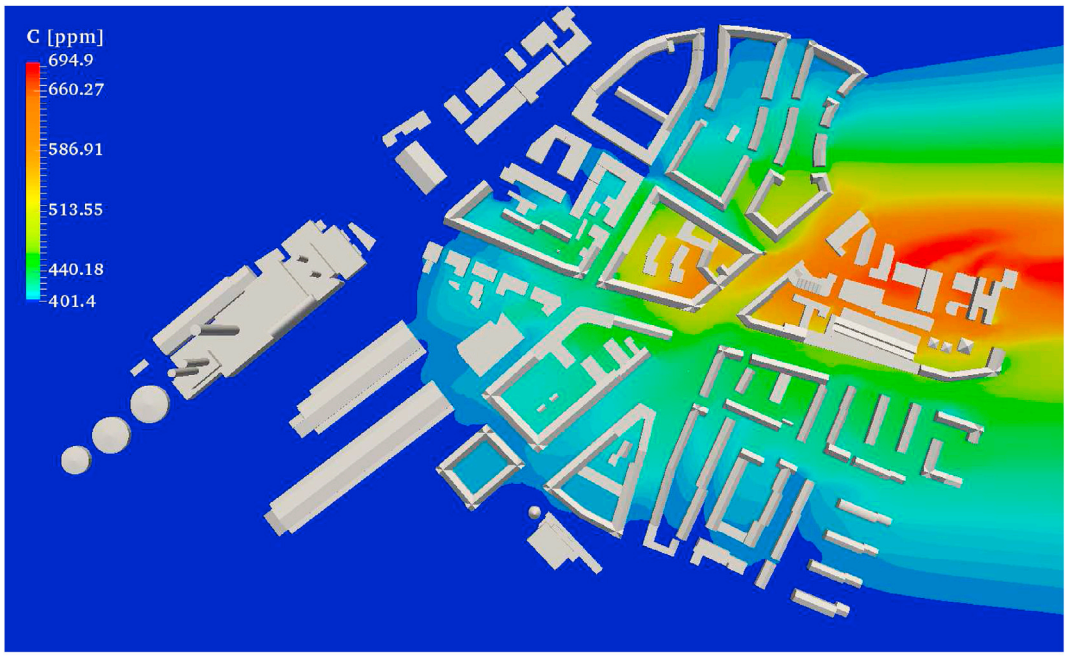

(a) Horizontal slice of C at $z = 4$m

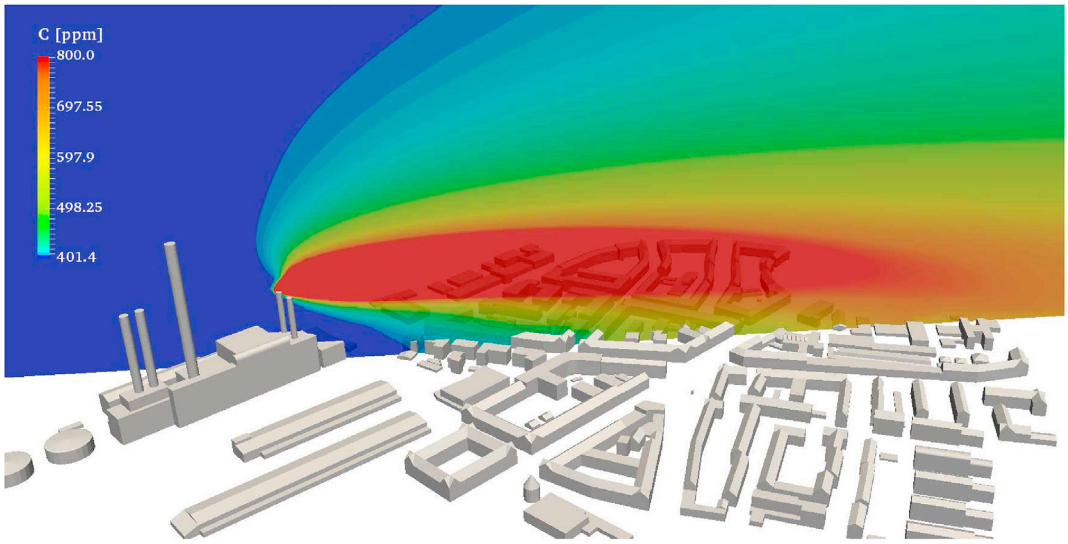

(b) Vertical slice of C

Fig. 16. Images of the CO_2 concentration.

observed in the street canyons at the left hand side of Fig. 17b, and the upstream effect is observed in the rest of the street canyons. It is also shown that the surrounding ground level is strongly affected downstream, since the neighbouring surface area reaches values higher than 403 ppm at a distance above 50 m from the power plant.

3.5. Improvement of the Gaussian model for the urban environment

As stated above, the Gaussian equation is not applicable to every actual ambient situation and the dispersion parameters have to been derived from actual atmospheric diffusion experiments (Seinfeld and Pandis, 2006). In the present investigation, we performed a numerical experiment (using CFD tools) and compared the results with XCO_2 field measurements.

The simulation results were compared with the Gaussian plume model presented in the literature and, after a parametrization iteration, we propose a new formula for computing the vertical dispersion parameter:

$$\sigma_z^{general} = 0.11x(1 + 0.0003x)^{-\frac{1}{2}}. \tag{22}$$

As is shown in Fig. 18, the new parametrization using Eq. (22) shows a better agreement with the numerical experiment results. However, it is observed that the Gaussian plume model does not reproduce accurately the gas concentration in an urban environment. Especially, the gas concentration is clearly overestimated near the ground. Therefore, we suggest an additional parametrization for being used when the near ground ($z \leq 40$ m) gas concentration needs to be computed:

$$\sigma_z^{ground} = 0.088x(1 + 0.0003x)^{-\frac{1}{2}}. \tag{23}$$

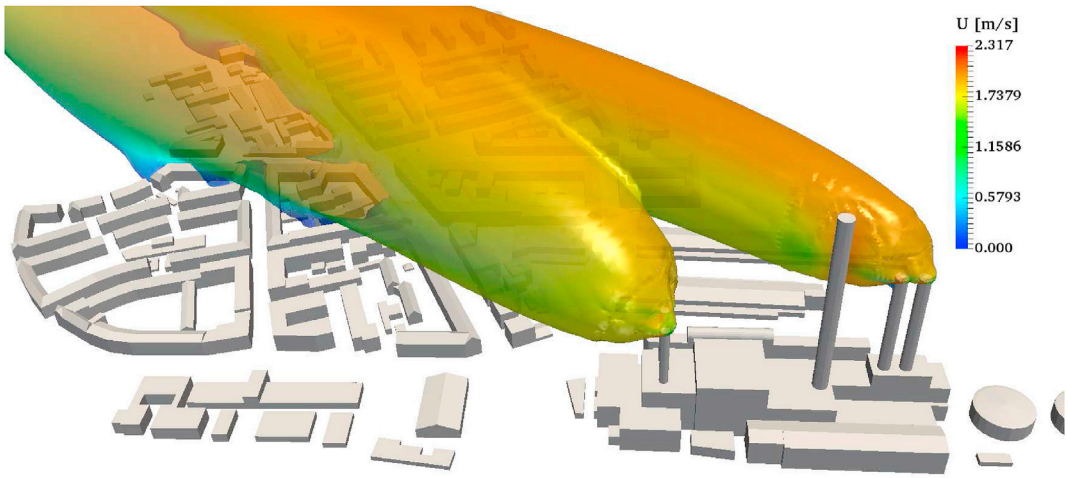

(a) Isosurface corresponding to $C = 500$ppm

(b) Isosurface corresponding to $C = 403$ppm

Fig. 17. Isosurfaces of CO_2 concentration.

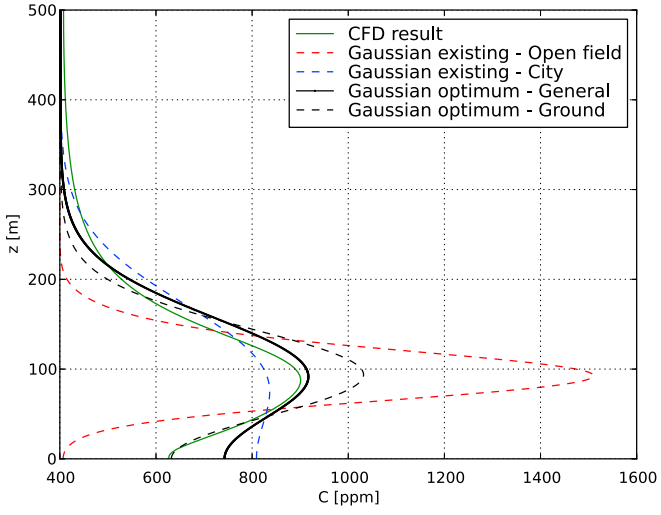

Fig. 18. Comparison for the urban case between XCO_2 simulation results and the Gaussian plume model using the optimum vertical dispersion parameter $\sigma_z(x)$ obtained empirically in the present investigation.

4. Conclusions

This investigation presents CFD simulations of CO_2 dispersion from a natural gas-fueled thermal power plant in an urban environment. This is the first time that CFD simulation results are compared with experimental measurements of XCO_2 on the site. A good agreement was obtained, yielding absolute and relative deviations of -0.05 ppm and 0.01%, respectively. This simulation error is one order of magnitude lower than the measurement error. Solution verification was also carried out by testing the convergence using 6 different mesh grid sizes.

Different turbulent Schmidt numbers were compared, and $Sc_t = 0.6$ was identified as the most adequate for being used in CFD simulations of CO_2 emissions from power plants in urban areas. Values in the range of $Sc_t = 0.5 - 0.8$ also show reasonably good results. These values yield an increase of the turbulent eddy dissipation (i.e. the gas diffusion) that compensates the underestimation of the turbulent kinetic energy computed. Apart from computational issues, in a real urban environment there are additional factors not considered in the simulations that increase the TKE (e.g. traffic).

The simulation results were also compared with the Gaussian plume model and a new parametrization, based on our simulation results, is suggested for being used in the urban environment. In particular, a new

formula for the vertical dispersion parameter is proposed. Since the gas concentration is overestimated close to the surface ($z < 40$ m), an additional expression is suggested for computing concentrations on the ground level. As further investigations, a wider study considering different distances from the emission source (and different case studies with different building configurations) would be interesting in order to verify the general applicability of the proposed formula. The Gaussian plume model can be continuously improved by analyzing different cases, and using different turbulence modeling approaches (i.e. RANS and LES).

The particular characteristics of the XCO_2 measurement were analyzed and taken into account for the comparison with simulation results. In particular, the influence of the measurement angles (i.e. azimuth and elevation) was found as determinant. The inclination angle of the column measurement must be considered in the design of future measurement campaigns.

Additionally, CO_2 concentration maps for the urban area were presented and analyzed. A high influence on the surroundings is observed, also at the ground level. Therefore, using also in-situ measurements of CO_2 concentration on the ground would be interesting for further investigations. The simultaneous use of multiple measurement techniques (e.g. column, surface, drones) may be of interest in order to carry out an extensive validation of the simulation domain, strengthening the conclusions derived from the simulation results.

It is demonstrated that CFD can be used as a powerful tool for simulating atmospheric greenhouse gas dispersion. In order to apply the computational tool, it would be interesting to perform more simulations and experimental measurements with other situations (e.g. measurement axis crossing the exhaust plume over a chimney). We use RANS turbulence modeling in the present investigation, but we want to express the interest in also using LES modeling in further research in order to compare the results obtained for real urban atmospheric environments using both methodologies.

Acknowledgements

Francisco Toja-Silva and Jia Chen are supported by Technische Universität München - Institute for Advanced Study, funded by the German Excellence Initiative and the European Union Seventh Framework Programme under grant agreement n° 291763.

The authors gratefully acknowledge former master students Hai Nguyen and Ludwig Heinle for preparing and performing the column measurements on the open field site. Markus Schmid and Dr. Mathias Müller from Fos4X are acknowledged for helping with the logistics. Prof. Steve Wofsy is also acknowledged for his advice.

The authors acknowledge the computer time provided by the Linux Cluster at the Leibniz Supercomputing Centre (Leibniz-Rechenzentrum, LRZ) of the Bavarian Academy of Sciences and Humanities.

The authors also gratefully acknowledge Stadtwerke München GmbH (SWM) for kindly providing power plant operational data and for their support, which has been essential for the success of this investigation.

We also acknowledge Zhu Ying and Dr. Mark Wenig from Ludwig-Maximilians-Universität München (LMU) for providing the wind data.

References

Architectural Institute Japan (AIJ), 2016. AIJ Benchmarks for Validation of CFD Simulations Applied to Pedestrian Wind Environment Around Buildings. ISBN978-4-8189-5001-6.

Beck, V., Koch, T., Kretschmer, R., Marshall, J., Ahmadov, R., Gerbig, C., Pillai, D., Heimann, M., 2011. The WRF Greenhouse Gas Model (WRF-GHG). Technical Report No. 25. Max Planck Institute for Biogeochemistry, Jena (Germany).

Blocken, B., Stathopoulos, T., Carmeliet, J., 2007. CFD simulation of the atmospheric boundary layer: wall function problems. Atmos. Environ. 41, 238–252.

Briggs, G.A., 1973. Diffusion Estimation for Small Emissions. ATDL Contribution File 79. Atmospheric Turbulence and Diffusion Laboratory.

Chen, J., Viatte, C., Hedelius, J.K., Jones, T., Franklin, J.E., Parker, H., Gottlieb, E.W., Wennberg, P.O., Dubey, M.K., Wofsy, S.C., 2016. Differential column measurements using compact solar-tracking spectrometers. Atmos. Chem. Phys. 16, 8479–8498.

Chen, J., Nguyen, H., Toja-Silva, F., Heinle, L., Hase, F., Butz, A., 2017. Power plant emission monitoring in Munich using differential column measurements. EGU General Assem. Conf. Abstr. 19, 16423.

Cheng, Y., Lien, F.S., Yee, E., Sinclair, R., 2003. A comparison of Large Eddy Simulations with a standard $k-\varepsilon$ Reynolds-Averaged Navier-Stokes model for the prediction of a fully developed turbulent flow over a matrix of cubes. J. Wind Eng. Ind. Aerodyn. 91, 1301–1328.

Durbin, P.A., 1996. On the $k-\varepsilon$ stagnation point anomaly. Int. J. Heat Fluid Flow 17, 89–90.

United States Environmental Protection Agency, 1980. OAQPS Guideline Series: Guidelines on Air Quality Models. Research Triangle Park.

Web: European Commission, climate change consequences. http://ec.europa.eu/clima/change/consequences_en (Accessed on 11 January 2017).

European Environmental Agency, 2012. Climate Change, Impacts and Vulnerability in Europe 2012. Office for Official Publications of the European Union, Luxembourg.

Web: European Union societal challenges. https://ec.europa.eu/programmes/horizon2020/en/h2020-section/societal-challenges (Accessed on 11 January 2017).

Feng, S., Lauvaux, T., Newman, S., Rao, P., Ahmadov, R., Deng, A., Díaz-Isaac, L.I., Duren, R.M., Fischer, M.L., Gerbig, C., Gurney, K.R., Huang, J., Jeong, S., Li, Z., Miller, C.E., O'Keeffe, D., Patarasuk, R., Sander, S.P., Song, Y., Wong, K.W., Yung, Y.L., 2016. Los Angeles megacity: a high-resolution land-atmosphere modelling system for urban CO_2 emissions. Atmos. Chem. Phys. 16, 9019–9045.

Ferziger, J.H., Perić, M., 2002. Computational Methods for Fluid Dynamics, third ed. Springer.

Franke, J., Hellsten, A., Schlnzen, H., Carissimo, B., 2007. Best Practice Guideline for the CFD Simulation of Flows in the Urban Environment. COST Action 732. COST Office, Brussels.

Frey, M., Hase, F., Blumenstock, T., Groβ, J., Kiel, M., Mengistu Tsidu, G., Schäfer, K., Sha, M.K., Orphal, J., 2015. Calibration and instrumental line shape characterization of a set of portable FTIR spectrometers for detecting greenhouse gas emissions. Atmos. Meas. Tech. 8, 3047–3057.

Gisi, M., Hase, F., Dohe, S., Blumenstock, T., Simon, A., Keens, A., 2012. XCO_2-measurements with a tabletop FTS using solar absorption spectroscopy. Atmos. Meas. Tech. 5, 2969–2980.

Web: Google Maps. COWI, GeoBasis-DE/BKG. https://www.google.de/maps/@48.0980986,11.5528472,1678a,20y,41.1t/data=!3m1!1e3 (Accessed on 1 March 2017).

Gromke, C., Blocken, B., 2015. Influence of avenue-trees on air quality at the urban neighborhood scale. Part I: quality assurance studies and turbulent Schmidt number analysis for RANS CFD simulations. Environ. Pollut. 196, 214–223.

Web: Guidebook for practical applications of CFD to pedestrian wind environment around buildings. Architectural Institute of Japan. http://www.aij.or.jp/jpn/publish/cfdguide/index_e.htm (Accessed on 17 May 2017).

Gurney, K.R., 2013. Beyond hammers and nails: mitigating and verifying greenhouse gas emissions. EOS 94, 199.

Gurney, K.R., Romero-Lankao, P., Seto, K.C., Hutyra, L.R., Duren, R., Kennedy, C., Grimm, N.B., Ehleringer, J.R., Marcotullio, P., Hughes, S., Pincetl, S., Chester, M.V., Runfola, D.M., Feddema, J.J., Sperling, J., 2015. Climate change: track urban emissions on a human scale. Nature 525, 179–181.

Hang, J., Li, Y., Sandberg, M., Buccolieri, R., Di Sabatino, S., 2012. The influence of building height variability on pollutant dispersion and pedestrian ventilation in idealized high-rise urban areas. Build. Environ. 56, 346–360.

Hanna, S.R., Briggs, G.A., Hosker, R.P., 1982. Handbook on Atmospheric Diffusion. U. S. Department of Energy.

Hanna, S.R., Brown, M.J., Camelli, F.E., Chan, S.T., Coirier, W.J., Hansen, O.R., Huber, A.H., Kim, S., Reynolds, R.M., 2006. Detailed simulations of atmospheric flow and dispersion in downtown Manhattan. An application of five computational fluid dynamics models. Bull. Am. Meteorol. Soc. 87, 1713–1726.

Hase, F., Frey, M., Blumenstock, T., Groβ, J., Kiel, M., Kohlhepp, R., Mengistu Tsidu, G., Schäfer, K., Sha, M.K., Orphal, J., 2015. Application of portable FTIR spectrometers for detecting greenhouse gas emissions of the major city Berlin. Atmos. Meas. Tech. 8, 3059–3068.

Hedelius, J.K., Viatte, C., Wunch, D., Roehl, C.M., Toon, G.C., Chen, J., Jones, T., Wofsy, S.C., Franklin, J.E., Parker, H., Dubey, M.K., Wennberg, P.O., 2016. Assessment of errors and biases in retrievals of XCO_2, XCH_4, XCO, and XN_2O from a 0.5 cm^{-1} resolution solar-viewing spectrometer. Atmos. Meas. Tech. 9, 3527–3546.

Web: IPCC's Task Force on National Greenhouse Gas Inventories. http://www.ipcc-nggip.iges.or.jp/(Accessed on 11 January 2017).

Jeanjean, A.P.R., Hinchliffe, G., McMullan, W.A., Monks, P.S., Leigh, R.J., 2015. A CFD study on the effectiveness of trees to disperse road traffic emissions at a city scale. Atmos. Environ. 120, 1–14.

Karion, A., Sweeney, C., Wolter, S., Newberger, T., Chen, H., Andrews, A., Kofler, J., Neff, D., Tans, P., 2013. Long-term greenhouse gas measurements from aircraft. Atmos. Meas. Tech. 6, 511–526.

Lary, D.J., Alavi, A.H., Gandomi, A.H., Walker, A.L., 2016. Machine learning in geosciences and remote sensing. Geosci. Front. 7, 3–10.

Lateb, M., Meroney, R.N., Yataghene, M., Fellouah, H., Saleh, F., Boufade, M.C., 2016. On the use of numerical modelling for near-field pollutant dispersion in urban environments - a review. Environ. Pollut. 208, 271–283.

Launder, B.E., Kato, M., 1993. Modeling flow-induced oscillations in turbulent flow around a square cylinder. In: ASME Fluid Engineering Conference.

Leuenberger, M., Kanevski, M., 2015. Extreme learning machines for spatial environmental data. Comput. Geosci. 85, 64–73.
Lide, D.R., 2004. CRC Handbook of Chemistry and Physics, 85th edition. CRC Press.
Web: Linux Cluster at the Leibniz Supercomputing Centre (Leibniz-Rechenzentrum, LRZ) of the Bavarian Academy of Sciences and Humanities. https://www.lrz.de/services/compute/linux-cluster/(Accessed on 27 February 2017).
Mays, K.L., Shepson, P.B., Stirm, B.H., Karion, A., Sweeney, C., Gurney, K.R., 2009. Aircraft-based measurements of the carbon footprint of Indianapolis. Environ. Sci. Technol. 43, 7816–7823.
McKain, K., Wofsy, S.C., Nehrkorn, T., Eluszkiewicz, J., Ehleringer, J.R., Stephens, B.B., 2012. Assessment of ground-based atmospheric observations for verification of greenhouse gas emissions from an urban region. Proc. Natl. Acad. Sci. U. S. A. (PNAS) 109, 8423–8428.
McKain, K., Down, A., Raciti, S.M., Budney, J., Hutyra, L.R., Floerchinger, C., Herndon, S.C., Nehrkorn, T., Zahniser, M.S., Jackson, R.B., Phillips, N., Wofsy, S.C., 2015. Methane emissions from natural gas infrastructure and use in the urban region of Boston, Massachusetts. Proc. Natl. Acad. Sci. U. S. A. (PNAS) 112, 1941–1946.
Meng, T., Hibi, K., 1998. Turbulent measurements of the flow field around a high-rise building. J. Wind Eng. (in Japanese) 76, 55–64.
Meroney, R., Ohba, R., Leitl, B., Kondo, H., Grawe, D., Tominaga, Y., 2016. Review of CFD guidelines for dispersion modeling. Fluids 1, 1–15.
Web: NASA, Megacities Carbon Project. https://megacities.jpl.nasa.gov/portal/about/ (Accessed on 11 January 2017).
Nozu, T., Tamura, T., 2012. LES of turbulent wind and gas dispersion in a city. J. Wind Eng. Ind. Aerodyn. 104–106, 492–499.
Web: OpenFOAM. http://www.openfoam.org (Accessed on 23 December 2016).
O'Sullivan, J.P., Archer, R.A., Flay, R.G.J., 2011. Consistent boundary conditions for flows within the atmospheric boundary layer. J. Wind Eng. Ind. Aerodyn. 99, 65–77.
Parente, A., Gorlé, C., van Beeck, J., Benocci, C., 2011. A comprehensive modelling approach for the neutral atmospheric boundary layer: consistent inflow conditions, wall function and turbulence model. Bound. Layer Meteorol. 140, 411–428.
Patnaik, G., Boris, J.P., Young, T.R., 2007. Large scale urban contaminant transport simulations with Miles. J. Fluids Eng. 129, 1524–1532.
Web: Pipe Flow Calculation, flue gases properties table. http://www.pipeflowcalculations.com/tables/flue-gas.php (Accessed on 13 January 2017).
Reynolds, R.M., 1992. ALOHA 5.0: Theoretical Discussion. Technical memorandum NOS ORCA-65. National Oceanic and Atmospheric Administration, Seattle, WA.
Richards, P.J., Hoxey, R.P., 1993. Appropriate boundary conditions for computational wind engineering models using the $k-\varepsilon$ turbulence model. J. Wind Eng. Ind. Aerodyn. 46–47, 145–153.
Seinfeld, J.H., Pandis, S.N., 2006. Atmospheric Chemistry and Physics: from Air Pollution to Climate Change. John Wiley & Sons.
Shen, H.H., Cheng, A.H.D., Wang, K.-H., Teng, M.H., Liu, C.C.K., 2002. Environmental Fluid Mechanics: Theories and Applications. ASCE Publications.
Web: SnappyHexMesh, OpenFOAM Wiki. http://openfoamwiki.net/index.php/SnappyHexMesh (Accessed on 23 December 2016).
Web: Stadtwerke München GmbH (SWM). https://www.swm.de/english.html (Accessed on 18 January 2017).
Sumner, J., Watters, C.S., Masson, C., 2010. CFD in wind energy: the virtual, multiscale wind tunnel. Energies 3, 989–1013.
Takano, Y., Moonen, P., 2013. On the influence of roof shape on flow and dispersion in an urban street canyon. J. Wind Eng. Ind. Aerodyn. 123, 107–120.
Tang, W., Huber, A., Bell, B., Schwarz, W., 2006. Application of CFD simulations for short-range atmospheric dispersion over open fields and within arrays of buildings. In: AMS 14th Joint Conference on the Applications of Air Pollution Meteorology with the A&WMA, Atlanta, GA (USA).
Toja-Silva, F., Peralta, C., Lopez, O., Navarro, J., Cruz, I., 2015. Roof region dependent wind potential assessment with different RANS turbulence models. J. Wind Eng. Ind. Aerodyn. 142, 258–271.
Toja-Silva, F., Peralta, C., Lopez-Garcia, O., Navarro, J., Cruz, I., 2015. Effect of roof-mounted solar panels on the wind energy exploitation on high-rise buildings. J. Wind Eng. Ind. Aerodyn. 145, 123–138.
Tominaga, Y., Stathopoulos, T., 2007. Turbulent Schmidt numbers for CFD analysis with various types of flowfield. Atmos. Environ. 41, 8091–8099.
Tominaga, Y., Stathopoulos, T., 2010. Numerical simulation of dispersion around an isolated cubic building: model evaluation of RANS and LES. Build. Environ. 45, 2231–2239.
Tominaga, Y., Stathopoulos, T., 2013. CFD simulation of near-field pollutant dispersion in the urban environment: a review of current modeling techniques. Atmos. Environ. 79, 716–730.
Tominaga, Y., Stathopoulos, T., 2016. Ten questions concerning modeling of near-field pollutant dispersion in the built environment. Build. Environ. 105, 390–402.
Tominaga, Y., Mochida, A., Murakami, S., Sawaki, S., 2008. Comparison of various revised $k-\varepsilon$ models and LES applied to flow around a high-rise building model with 1:1:2 shape placed within the surface boundary layer. J. Wind Eng. Ind. Aerodyn. 96, 389–411.
Tsuchiya, M., Murakami, S., Mochida, A., Kondo, K., Ishida, Y., 1997. Development of a new $k-\varepsilon$ model for flow and pressure fields around bluff body. J. Wind Eng. Ind. Aerodyn. 67–68, 169–182.
van Hooff, T., Blocken, B., 2010. On the effect of wind direction and urban surroundings on natural ventilation of a large semi-enclosed stadium. Comput. Fluids 39, 1146–1155.
Wingstedt, E.M.M., Osnes, A.N., Åkervik, E., Eriksson, D., Pettersson Reif, B.A., 2017. Large-eddy simulation of dense gas dispersion over a simplified urban area. Atmos. Environ. 152, 605–616.
Wunch, D., Toon, G.C., Blavier, J.-F.L., Washenfelder, R.A., Notholt, J., Connor, B.J., Griffith, D.W.T., Sherlock, V., Wennberg, P.O., 2011. The total carbon column observing network. Philos. Trans. R. Soc. A 369, 2087–2112.
Yap, C.J., 1987. Turbulent Heat and Momentum Transfer in Recirculating and Impinging Flows. PhD Thesis. Faculty of Technology, University of Manchester, United Kingdom.
Yoshie, R., Mochida, A., Tominaga, Y., Kataoka, H., Harimoto, K., Nozu, T., Shirasawa, T., 2007. Cooperative project for CFD prediction of pedestrian wind environment in the Architectural Institute of Japan. J. Wind Eng. Ind. Aerodyn. 95, 1551–1578.
Yu, H., Thé, J., 2016. Validation and optimization of SST $k-\omega$ turbulence model for pollutant dispersion within a building array. Atmos. Environ. 145, 225–238.
Yue, T.X., Zhang, L.L., Zhao, M.W., Wang, Y.F., Wilson, J., 2016. Space- and ground-based CO_2 measurements: a review. Sci. China Earth Sci. 59, 2089–2097.
Zeebe, R.E., Ridgwell, A., Zachos, J.C., 2016. Anthropogenic carbon release rate unprecedented during the past 66 million years. Nat. Geosci. 9, 325–329.
Zhang, Y., Kwok, K.C.S., Liu, X.-P., Niu, J.-L., 2015. Characteristics of air pollutant dispersion around a high-rise building. Environ. Pollut. 204, 280–288.